Assisted Peptide Folding by Surface Pattern Recognition

Zhuoyun Zhuang,[†△] Andrew I. Jewett,[†△] Silvan Kuttimalai,[†] Giovanni Bellesia,[§] S. Gnanakaran,[§] and Joan-Emma Shea[†‡*]

[†]Department of Chemistry and Biochemistry, and [‡]Department of Physics, University of California, Santa Barbara, California; and [§]Center for Nonlinear Studies, Theoretical Division, Los Alamos National Laboratory, Los Alamos, New Mexico

ABSTRACT Natively disordered proteins belong to a unique class of biomolecules whose function is related to their flexibility and their ability to adopt desired conformations upon binding to substrates. In some cases these proteins can bind multiple partners, which can lead to distinct structures and promiscuity in functions. In other words, the capacity to recognize molecular patterns on the substrate is often essential for the folding and function of intrinsically disordered proteins. Biomolecular pattern recognition is extremely relevant both in vivo (e.g., for oligomerization, immune response, induced folding, substrate binding, and molecular switches) and in vitro (e.g., for biosensing, catalysis, chromatography, and implantation). Here, we use a minimalist computational model system to investigate how polar/nonpolar patterns on a surface can induce the folding of an otherwise unstructured peptide. We show that a model peptide that exists in the bulk as a molten globular state consisting of many interconverting structures can fold into either a helix-coil-helix or an extended helix structure in the presence of a complementary designed patterned surface at low hydrophobicity (3.7%) or a uniform surface at high hydrophobicity (50%). However, we find that a carefully chosen surface pattern can bind to and catalyze the folding of a natively unfolded protein much more readily or effectively than a surface with a noncomplementary or uniform distribution of hydrophobic residues.

INTRODUCTION

Proteins have a remarkable capacity to interact with many molecular species, including other proteins/peptides, lipid membranes, Teflon, silica, polystyrene, and a variety of medical implants. In many instances, the presence of these additional bodies is necessary for folding to occur. Natively unstructured (also known as natively or intrinsically disordered or unfolded) proteins are a class of proteins that only adopt (or for which part of the protein adopts) a well-defined structure upon binding to a substrate. Proteins belonging to this class play a wide variety of roles in the body, ranging from cell signaling and regulation to molecular assembly in the form of functional oligomers or toxic aggregates. Examples of proteins that are either partially or fully disordered include casein, prion protein (PrP), p53, p21, p27, synuclein, and certain classes of antimicrobial polymers (1–6).

The adoption of a fold (and thus function) can be mediated through the process of pattern recognition. Pattern recognition by proteins is relevant in many contexts and involves oligomer assembly, immune response, induced folding and unfolding, enzyme/substrate interactions, and molecular switches. It is also gaining importance in the field of biotechnology (e.g., biosensing, catalysis, chromatography, and implantation) (7). For instance, the observation that naturally occurring enzymes under denaturating conditions are able to recover their function and fold in the presence of their substrates (8) led to the engineering of natively unfolded enzymes (via mutation of truncation) that can only reach their functional fold in the presence of a substrate. These enzymes form the basis of a new class of highly specific biosensors (9–11). Another class of biosensors that make use of pattern recognition takes advantage of the intrinsically unstable nature of short peptides (11–14). Of interest, although some intrinsically disordered peptides bind only to one partner, for others (as in the case of p53), pattern recognition can lead to binding to different partners, resulting in distinct structures and promiscuity in functions (5,15).

In this work, we sought to understand how a natively disordered peptide can adopt a well-defined fold via surface pattern recognition. Although much theoretical and experimental work has focused on the adsorption of natively structured proteins on surfaces, and the resulting conformational change, stabilization, or destabilization (16–21), little effort has been made to understand how surfaces can impact the structure of natively disordered proteins. Using a coarse-grained representation of the protein and molecular-dynamics simulations, we explored the behavior of two model peptides (a natively disordered peptide and a natively structured peptide) in the bulk and on various patterned surfaces. The natively structured peptide is a stable, two-stranded β-hairpin (obtained by truncating a four-strand β barrel at the central turn; Fig. 1). Small, two-strand β-hairpins are a common motif in larger proteins and can be stable in isolation (22–25). The natively disordered peptide is obtained by truncation of a four-helix bundle with a sequence based on a protein designed by Hecht and co-workers (26–28). The original Hecht protein consists of

Submitted September 22, 2010, and accepted for publication December 21, 2010.

[△]Zhuoyun Zhuang and Andrew I. Jewett contributed equally to this work.

*Correspondence: shea@chem.ucsb.edu

Editor: Ruth Nussinov.

0006-3495/11/03/1306/10 $2.00

doi: 10.1016/j.bpj.2010.12.3735

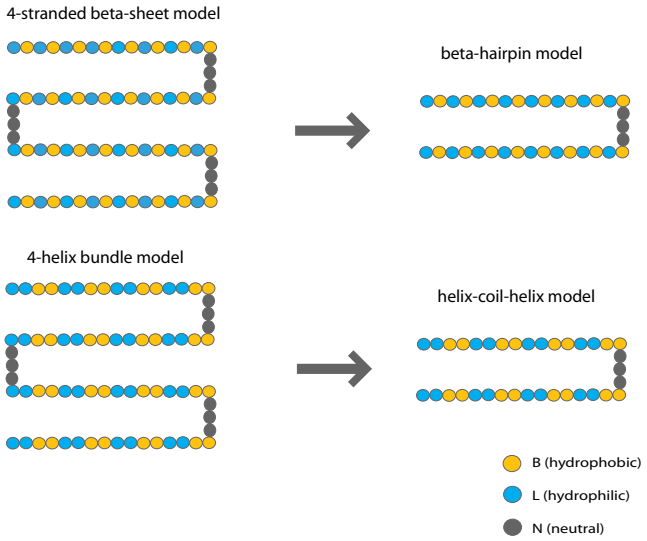

FIGURE 1 The sequence of the β-hairpin model (LB LB LB LB LB LB LB NNN BL BL BL BL BL BL BL BL) is based on the BF peptide used by Bellesia et al. (34). The β-hairpin model is a truncation of the original larger four-stranded β-barrel. The sequence of the helix-coil-helix (LL BB LL BB LL BB LL BB NNN BB LL BB LL BB LL BB LL) is based on the AUF2 sequence used by Bellesia et al. (34). The original four-helix bundle is truncated in half into a helix-coil-helix.

four helices (see Fig. 1). In principle, there are two different ways to truncate the four-helix bundle. Truncation of the central turn leads to two helix-coil-helix motifs, whereas truncation at all three turn regions leads to four single-helix motifs. In isolation, the single helix is unstructured (28). Helix-coil-helices also tend to be unstable, and only one successfully designed model system is reported in the literature (29). However, both of these truncated peptides can regain structure upon association, as evidenced by circular dichroism and NMR experiments in which oligomerization (dimerization or tetramerization) led to the formation of well-structured four-helix bundles (28,30). This process allows stabilization of the secondary structure because the hydrophobic residues, which are otherwise exposed in the monomer, are effectively buried. Here, we use as our model for a natively disordered peptide the peptide obtained by truncating the four-helix bundle at the central turn. We refer to this peptide as the helix-coil-helix model, although this peptide in fact resembles a molten globule in the bulk consisting of many interconverting structures. Even in its unstructured state, our peptide has high helical content. In contrast, naturally existing, intrinsically disordered peptides may have low secondary structure content in their natively unfolded states (due in large part to the high charge/low hydrophobicity of their sequences). However, our helix-coil-helix model and intrinsically disordered peptides share a common feature in that they are not able to adopt well-defined stable conformation in the bulk and they require a binding partner to fold. In this study, we address the following questions: How do surfaces induce structure in natively disordered proteins? Is it possible to control tertiary arrangements through the use of explicit surface patterns? The latter question is particularly relevant in light of the experimental observation that certain intrinsically disordered peptides can bind to several different partners and yield distinct folded structures (5,15,31–33).

MATERIALS AND METHODS

Peptide model

In this study we used an off-lattice peptide to investigate the effect of patterned surfaces on folding. Specifically, we were interested in determining how surface pattern recognition might assist folding. To that end, we considered two different peptides: a helix-coil-helix and a β-hairpin. Both are truncated versions of larger peptides, i.e., the four-helix bundle and the four-strand β-barrel studied by Bellesia et al. (34).

As in the Honeycutt-Thirumalai model (35–37), each monomer/amino acid is represented as a single bead, which can be hydrophobic (B), hydrophilic (L), or neutral (N). A Lennard-Jones potential is used to describe interactions between nonbonded beads: $U_{nb}(r_{ij}) = 4\varepsilon[(\sigma/r_{ij})^{12} - \lambda_{ij}(\sigma/r_{ij})^{6}]$, where r_{ij} is the distance between beads i and j ($|j - i| > 2$), σ is the bead diameter (~3.8 Å), ε is the increase in stability that results from bringing two hydrophobic amino acids together (estimated at 1–3 kcal/mole) (34,38–41), and $\lambda_{ij} = 1.0$ if both residues i and j are hydrophobic (B), and zero otherwise. In this model, attractive forces exist only between pairs of nonbonded hydrophobic (B) residues. Hydrophilic (L) and neutral (N) beads interact with all other beads only through short-range (steric) repulsion. The only difference between L and N residues is their effect on secondary structure. N residues are located in turn regions and allow the chain to be more flexible due to weaker torsion-angle forces, whereas L and B residues have either helical or β torsion-angle forces (see below).

Harmonic forces are used to constrain bond lengths between successive Cα atoms in the chain, as well as bond angles: $U_{bond}(r) = K_b/2\ (r - r_0)^2$, and $U_{bangle}(\theta) = K_\theta/2\ (\theta - \theta_0)^2$, where $K_b = 100.0\ \varepsilon/\sigma^2$, $K_\theta = 13.33\ \varepsilon/\text{rad}^2$, $\theta_0 = 105°$, $r_0 = \sigma$, and σ and ε are as defined above.

We model the four-body torsion angle forces between four successive residues (ϕ) of type B or L in the chain using a potential function with two deep minima roughly at 60° and 180°, corresponding to α-helix and β-strand conformations. $U_{dihe}(\gamma) = C\ [\cos(3\gamma) + \cos(\gamma + \delta)]$, where $C = 1.2\ \varepsilon$ (see Fig. S1 in the Supporting Material). The torsion angle forces are discussed in more detail in Fig. S1 and Bellesia et al. (34).

Our helix-coil-helix is a truncated fragment of the AUF2 model used by Bellesia et al. (34), which was inspired by a variety of helix bundles that were studied extensively in experiments by the Hecht group (26–28) (Fig. 1). The sequence of our helix-coil-helix is LL BB LL BB LL BB LL BB NNN BB LL BB LL BB LL BB LL. In our study, the helix-coil-helix is biased toward helical conformations ($\delta = 65°$). The magnitude of this bias is consistent with amino acids with a high propensity for α-helix secondary structure. The β-hairpin is based on the BF peptide (unfrustrated/unbiased β model) used by Bellesia et al. (34) and has the sequence LB LB LB LB LB LB LB LB NNN BL BL BL BL BL BL BL BL. This β-hairpin model is able to fold in the bulk without using any torsional angle bias. Because bias was not needed, we used unbiased ($\delta = 60°$) torsion angle forces.

The de novo proteins on which these models are based are known to be unstable when cut into fragments. For example, although the original uncut four-helix bundle may be stable in the bulk, the single-helix fragments tend to exhibit random-coil-like CD spectra at low concentrations in the bulk (28). Consequently, our helix-coil-helix and β-hairpin models are expected to be less stable in the bulk than their larger counterparts (i.e., the four-helix bundle and four-sheet β-barrel model). In our study, when the helix-coil-helix model was simulated alone in the bulk (i.e., mimicking low concentration), it adopted random-coil conformations. However, the dimer simulations (mimicking high concentration) that were performed

by confining two helix-coil-helix models within a purely repulsive spherical barrier of radius 20σ (42) led to a well-defined, dimeric, four-helix bundle. This observation illustrates how the stability of the fragment can be restored by the presence of a complementary binding partner.

Surface model

For our simulation we use two types of surfaces: a continuous, homogeneous surface and an explicit, nonhomogeneous, patterned surface. The latter is constructed from the same type of beads used in the protein model, specifically the B and L beads. Peptide-surface interactions are modeled in similarity to intramolecular interactions in the peptide model so as to mimic generic attractive interactions such as the hydrophobic effect, the van der Waals force, and electrostatic interactions. Different surface patterns and degrees of hydrophobicity are implemented by varying the type of beads within the surface. For explicit surfaces, the hydrophobic composition (percent hydrophobicity) refers to the percentage of hydrophobic beads present within the surface.

In contrast, a continuous surface is composed of a mixture of B and L beads distributed uniformly with a density of one bead per σ^2 area ($\rho = 1/\sigma^2$). We implement hydrophobicity in the continuous surface using the variable h (between 0 and 1), where h represents the percentage of beads of type B within the surface. The remaining beads on the surface are of type L. We compute the interaction between the continuous surface and our peptide by adding up the interactions between each bead in the surface with each bead in our peptide. In this case, the beads are distributed uniformly on the XY plane, and consequently this sum is an integral over the XY plane. For each hydrophobic bead in the peptide (type B), the surface-interaction energy is:

$$U_{cont}(z) = 4\pi\,\varepsilon\,\rho\,\sigma^2\left((1/5)(\sigma/z)^{10} - (h/2)(\sigma/z)^4\right)$$

Where z is the distance of the peptide bead from the surface. Other beads in the peptide (type L and N) are not attracted to the surface, and consequently they lack the attractive $(\sigma/z)^4$ term. This $1/z^{10}$ and $1/z^4$ potential on the continuous surface is equivalent to the $1/r^{12}$ and $1/r^6$ interactions between the peptide and an explicit beaded surface (see Fig. S4). We establish boundary conditions by placing two identical parallel surfaces ~32 σ apart in the Z axis, which is larger than the radius of gyration of the completely unfolded peptide used in our simulation. The surfaces are then extended indefinitely in the X and Y directions.

Simulation and analysis methods

Replica exchange simulations (43–45) were performed on the helix-coil-helix and β-hairpin models in bulk and in the presence of surfaces. The temperature range was from 0.175 to 0.65 ε/k_BT. For each pair of neighboring temperatures, the acceptance ratio (the number of successful swaps divided by the number of swap attempts for that particular pair, i.e., the fraction of successful exchanges) was ~50–80%. The free-energy landscape for folding was characterized as follows: The free-energy map (sometimes called the potential of mean force) was plotted as a function of R_g (radius of gyration) and Xα (percentage of helical dihedral angle) at $T = 0.3$ (ε/k_B), where 0.3 (ε/k_B) is roughly the folding temperature for the helix-coil-helix on a number of continuous and explicit patterned surfaces (heat capacity data not shown). Torsion angles in the range of 29–109° were counted as helical (see Supporting Material for additional details). The weighted histogram analysis method (47–49) was used to calculate free-energy maps. Data from all temperatures were taken into account during the free-energy calculation. All simulations were initiated by placing the random unfolded peptide at least 10σ from the nearest surface. Simulations were performed using Langevin dynamics with a velocity decay rate of $\zeta = 0.04$ (in units of τ^{-1}, where τ is defined as the square root of ($m\sigma^2/\varepsilon$), and m is the mass of a typical amino acid). All energies are in units of ε and all distances are measured in units of σ.

RESULTS

Helix-coil-helix: an intrinsically unstable peptide

The helix-coil-helix is disordered in the absence of a favorable binding partner

To investigate how pattern recognition might assist/guide peptide folding, we performed replica exchange simulations of the helix-coil-helix monomer in the bulk and in the presence of both homogeneous surfaces and explicit surfaces with distinct patterns. For comparison, we also simulated the dimerization of two helix-coil-helices. Our results indicate that despite the built-in sequence and dihedral angle preference for helical bundle formation, the peptide model (as monomer) is disordered both in the bulk and in the presence of a purely repulsive surface. In both cases, the free-energy maps plotted as a function of the radius of gyration (R_g) and the helical content (Xα) show a single, broad basin centered around $R_g = 1.6\sigma$ and Xα = 77% (Fig. 2). The structures correspond to a variety of collapsed conformers (Fig. 2). Additional kinetics simulations at constant temperature demonstrated spontaneous and frequent transitions between these collapsed conformations (Fig. S2). These structures arise because the peptide is unable to effectively bury the hydrophobic residues to form a hydrophobic core while simultaneously forming short helices. On the other hand, we observe that two helix-coil-helices quickly dimerize with each other and form a stable four-helix bundle with anti-bisecting-U topology (30,50,51). Each monomer folds into a helix-coil-helix corresponding to a single prominent basin ($R_g = 2.9\sigma$, Xα = 92%) in the free-energy map (Fig. 2), where 92% Xα corresponds to ~24 helical torsion angles per monomer. Our simulation results are consistent with the experimental observation that secondary structures (helices) in small peptides are stabilized upon oligomerization (28).

A homogeneous surface induces folding of a disordered peptide into a helical structure

Simulations were performed with a homogeneous attractive surface of increasing hydrophobicity. The free-energy landscapes corresponding to these simulations are shown in Fig. 3. At 0% hydrophobicity (a purely repulsive surface), only the unfolded basin ($Rg = 1.9\sigma$, Xα = 77%) is populated. As hydrophobicity increases, a second basin starts to appear at a higher radius of gyration and helical content ($R_g = 2.9\sigma$, Xα = 92%). This basin corresponds to well-formed helix-coil-helices (denoted as bundle-R). Under 40% hydrophobicity ($h < 0.4$), the majority of the structures belong to the compact disordered basin. Above 40% hydrophobicity, the population gradually shifts from disordered structures to well-formed helix-coil-helices, with equal populations of both basins seen at the above locations ($R_g = 2.9\sigma$, Xα = 92%, or $R_g = 1.9\sigma$, Xα = 77%). The basin corresponding to disordered structures disappears completely at 60%

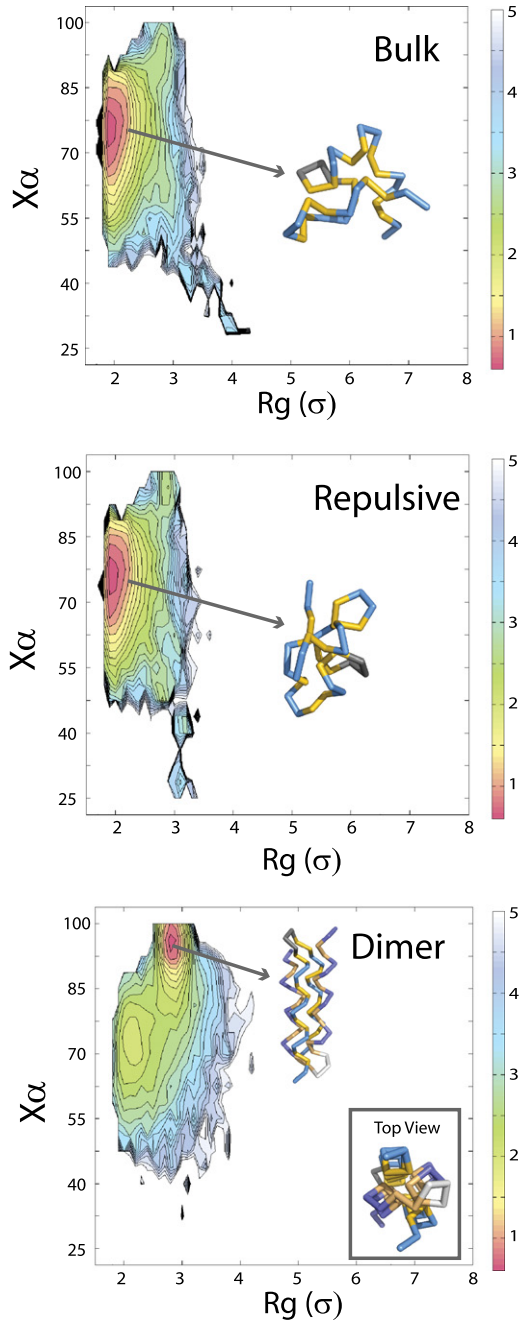

FIGURE 2 Free-energy maps for the helix-coil-helix monomer in the bulk (*top*), the monomer in the presence of repulsive surface (*middle*), and the dimer in the bulk (*bottom*). Free energies are plotted at T = 0.3 (ε/k_B). The X axis represents the radius of gyration (in units of σ), and the Y axis represents the percentage of helical dihedral angles Xα (Xα is the percentage of backbone dihedral angles in the range of 29–129°, excluding turns; 100% corresponds to 26 helical torsion angles). For the monomer (both in the bulk and in the presence of a repulsive surface), compact disordered structures dominate the population. For the dimer, a free-energy map is constructed with the same reaction coordinates, calculated separately for each monomer in the dimer simulation. The two monomers assemble to form a stable dimeric four-helix bundle. Each monomer adopts a helix-coil-helix conformation. Snapshots are shown next to the free-energy maps. For the peptide model, hydrophobic beads (B) are colored in yellow/wheat, neutral beads (N) are present only in the turn region and are colored in gray/white, and hydrophilic beads (L) are colored in blue/slate.

hydrophobicity (Fig. 3). For our model, the free-energy map remains the same when the hydrophobicity is increased from 60% to 100%. However, given the simplicity and limitations of our minimalist model, we prefer not to overinterpret the behavior of the peptide under such extreme conditions.

An explicit attractive patterned surface can induce a range of helical structures

We examined a number of patterns with various degrees of hydrophobicity (as measured by the percentage of hydrophobic/B residues on the surface).

A surface with low hydrophobicity induces folding via specific pattern recognition. The first pattern we studied was the $n \times 9$ pattern, where n corresponds to the total number of adjacent rows with hydrophobic beads, and 9 is the number of adjacent hydrophobic beads in a given row. In our study, n varied between 1 and 3. We initially focused on this pattern because the length of the pattern (nine beads) exactly matches the length of one helix of a perfect helix-coil-helix, making it a possible candidate to rescue the helix-coil-helix conformer via pattern recognition. On the 2×9 rectangle pattern (3.7% hydrophobic beads), two basins can be observed in the free-energy map (Fig. 4). One corresponds to a slightly expanded disordered conformer ($R_g = 2.5\sigma$ and X$\alpha = 77\%$), and the other corresponds to a helix-coil-helix ($R_g = 2.6\sigma$ and X$\alpha = 92\%$). When a 3×9 pattern (5.6% hydrophobic beads) is used, only a very small fraction of the peptides can fold to a helix-coil-helix, and the free-energy map shows that the major basin corresponds to unfolded structures with low helical content (Fig. 4). In contrast, a surface with two 1×9 hydrophobic stripes separated by a single repulsive stripe leads to a more pronounced basin for the helix-coil-helix.

The second class of patterns we studied was the $n \times$ infinity pattern. The $1 \times$ infinity pattern (5% hydrophobic beads) yielded a single basin in the free-energy map corresponding to disordered structures. The $2 \times$ infinity pattern (11% hydrophobic beads), on the other hand, exhibited a new basin at an extended R_g and high helical content ($R_g = 5.0 - 6.5\sigma$, X$\alpha = 92\%$) corresponding to an extended helical structure. We will refer to this structure as "stacked" to contrast it with the bundle structure. In addition to the extended helical structure, an extended structure with low helicity is seen. Two helical bundles are not observed for this pattern (Fig. 4). Finally, we studied patterns consisting of small hydrophobic patches (2×2 squares, 25% hydrophobic beads; Fig. 4). Such patterns did not yield either a bundle or a stacked helix structure, but led to a variety of disordered conformations.

Of note, it is not necessary for a patterned surface to have a large fraction of hydrophobic surface area to cause

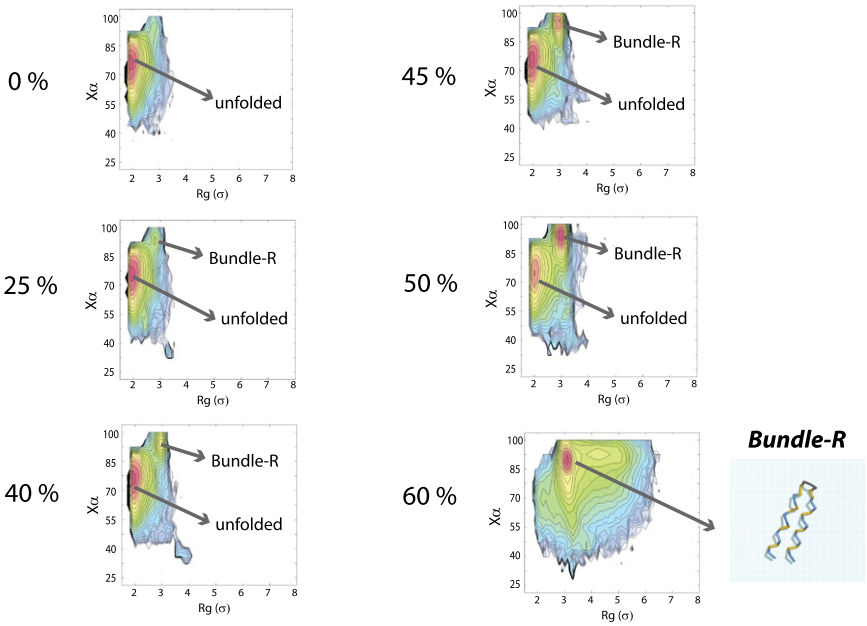

FIGURE 3 Free-energy maps of the helical model on a continuous surface at various hydrophobic fractions, h. Free energies are plotted at $T = 0.3$ (ε/k_B). When the overall hydrophobic fraction, h, is $\leq 40\%$, most structures are compact and disordered. At 45% hydrophobicity, the compact disordered structures are only slightly favored compared with the helix-coil-helices. At h = 50%, helix-coil-helices are slightly favored over the compact disordered structures. At h = 60%, helix-coil-helices are favored and the basin for compact disordered structures is completely absent. A snapshot for the helix-coil-helix (bundle-R) is shown. Similar results were observed for explicit surfaces (see Fig. S4).

a significant shift from disordered structures to structures with high helical content. In fact, only 3.7% and 11% of the beads are hydrophobic in the 2 × 9 rectangle pattern and the 2 × infinity stripe pattern, respectively. This is in agreement with our studies, which indicated that the peptide is more likely to see the local pattern on the surface instead of the overall hydrophobicity (E. Zhuang, A. I. Jewett, and J.-E. Shea, unpublished). Of more importance, we found that helix formation is extremely sensitive to the size of local hydrophobic patch: a 2 × 9 patch encourages helix formation, whereas a slightly larger patch (3 × 9 patch) disrupts helix formation. This result is consistent with a previous observation that the size of local hydrophobic patches is a relevant factor in governing helix formation (52).

We also observed that on surfaces with low hydrophobicity (<50%) and nonideal patterns (noticeably the 2 × 2 checkerboard or 1 × infinity single stripe), the peptide remains completely disordered (Fig. 4). It is important to point out that the 2 × 9 rectangle pattern and the 2 × infinity stripe pattern provide enough specificity for the peptide to fold into either a helix-coil-helix or two stacked helices (end-to-end), but not both. At the same time, the disordered population is still significant. It is possible that the overall hydrophobicity of these two surfaces is not sufficiently high, and/or the surface pattern does not perfectly complement the shape of a helix-coil-helix.

A surface with high hydrophobicity induces folding via nonspecific binding. We examined similar patterns at high hydrophobicity, with surprising results. We found that a checkerboard pattern consisting of alternating B and L beads can completely eliminate the disordered basin and strongly favor the formation of a helix-coil-helix (Fig. 5). When the 1 × infinity pattern is used at 50% hydrophobicity, the peptide now mostly folds into a helix-coil-helix with a hint of some stacked helix conformers (Fig. 5). This is in sharp contrast to the 1 × infinity striped pattern, which disfavors helical structures at low hydrophobicity (25% hydrophobic beads). The 2 × infinity pattern, which produces stacked helices at low hydrophobicity, continues to favor the stacked helical conformers at 50% hydrophobicity (Fig. 5). Of interest, a new basin corresponding to the helix-coil-helix also emerges for this pattern. Although the alternating B/L checkerboard pattern and the 1 × infinity pattern completely eliminate the unfolded population at high hydrophobicity, the 2 × infinity pattern is not able to do so. A close inspection of the helix-coil-helices formed on the continuous surfaces reveals that the hydrophobic residues on the peptide are packed differently compared with those formed on several of the explicit surfaces (see Discussion) (Fig. S5). Specifically, the packing between the two helices is tighter on these explicit surfaces (bundle-T). By comparison, the helix-coil-helix on the continuous surface is semi-flattened and shows more relaxed packing (bundle-R).

Surface-induced stabilization of an intrinsically stable β-hairpin

For comparison, we also explored the behavior of a stable peptide (with β-sheet secondary structure) in the vicinity of patterned and uniform surfaces. This particular peptide is stabilized in the presence of a uniform, continuous hydrophobic surface (h = 0.2…h = 1.0; Fig. S6). It is stabilized even more in the presence of an explicit 2 × 12 rectangular pattern, which mimics the interface provided by the other half of the four-sheet β-barrel. This is because, unlike a uniform surface, which sticks to both β-strands regardless

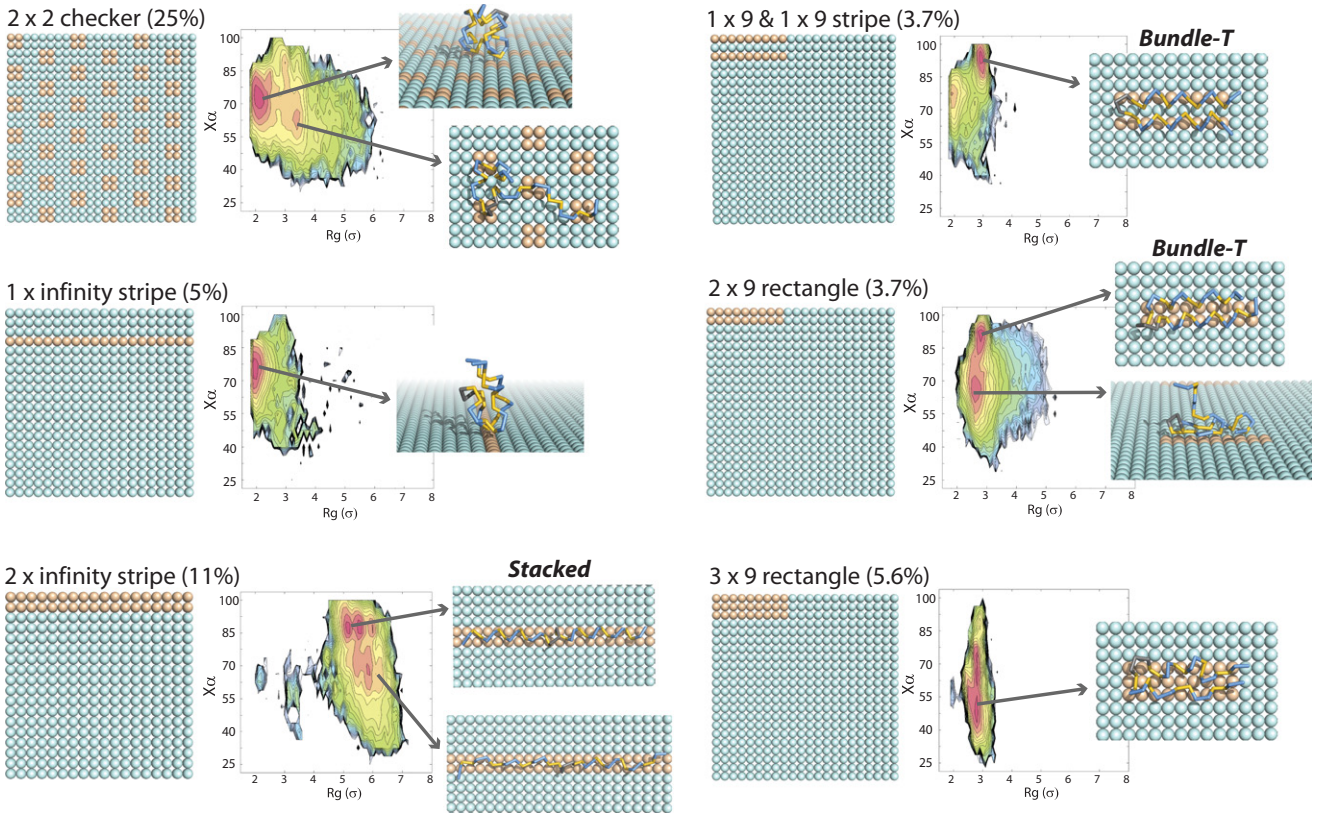

FIGURE 4 Explicit surface patterns with low hydrophobic composition (<50%) and their corresponding free-energy maps for the helical model. Free energies are plotted at T = 0.3 (ε/k_B). Surface hydrophobic beads (B) are colored in light brown. Surface hydrophilic beads (L) are colored in blue. The beads used on the surface are exactly the same as those found in the peptide model; they are colored a slightly different shade for contrast. For the peptide model, hydrophobic beads (B) are colored in yellow, neutral beads (N) are colored in gray, and hydrophilic beads (L) are colored in blue. Top left: 2 × 2 square patches arranged in a pattern consisting of 25% hydrophobic beads overall. A variety of compact disordered structures are observed. Middle left: 1 × infinity stripe pattern of 5% hydrophobic beads. Compact or semiextended disordered structures are observed. Bottom left: 2 × infinity stripe pattern at 11%. Extended disordered structures and stacked helical structures are observed. Top right: A 3.7% hydrophobic pattern consisting of two 1 × 9 & 1 × 9 stripes, separated by a single row of hydrophilic beads. The formation of helix-coil-helix is greatly favored. Middle right: A 2 × 9 rectangle pattern also at 3.7%. Semiextended disordered structures and helix-coil-helices are observed. Bottom right: A 3 × 9 rectangular pattern at 5.6%. Only semiextended disordered structures are observed. These structures have the overall shape of the helix-coil-helix but lack the well-formed helical turns. Snapshots are provided for significant minima seen on the free-energy landscape.

of their direction, the patterned surface only rewards conformations that have the correct tertiary structure, with the two β-strands antiparallel and side-by-side (Fig. S6).

DISCUSSION

In this work we investigated the behavior of small peptides/fragments of peptides. Such peptides lack a well-defined hydrophobic core and thus are more likely to be intrinsically disordered. In comparison, larger globular proteins have a well-defined/buried hydrophobic core. In our peptide models (the helix-coil-helix and β-hairpin), intramolecular interactions are not necessarily disrupted by peptide-surface interactions, i.e., there is very little competition between intra- and intermolecular interactions. However, this is not the case for large globular proteins. To be able to interact strongly with a hydrophobic surface, these larger proteins may have to disrupt a significant number of intramolecular interactions and expose their hydrophobic core. We suspect that a hydrophobic surface is more likely to destabilize large globular proteins (53,58–62) than small peptide fragments (or larger intrinsically disordered peptides, which we expect to behave similarly to the peptide fragments).

Our results suggest that a surface with the complementary pattern, even at low hydrophobicity (h $\leq$ 25%), can induce a well-defined structure in an otherwise unstructured peptide. The surface can recover and stabilize a peptide that is unstable in the absence of a binding partner. For instance, although the hydrophobic residues are fully protected in the four-helix bundle, they are exposed in the helix-coil-helix. Consequently, the helix-coil-helix is unable to fold on its own in the bulk. A surface with the right pattern can stabilize the helix-coil-helix by providing complementary interactions that are normally supplied by the other half of the four-helix bundle. In addition, the pattern of choice can also induce the peptide to adopt new

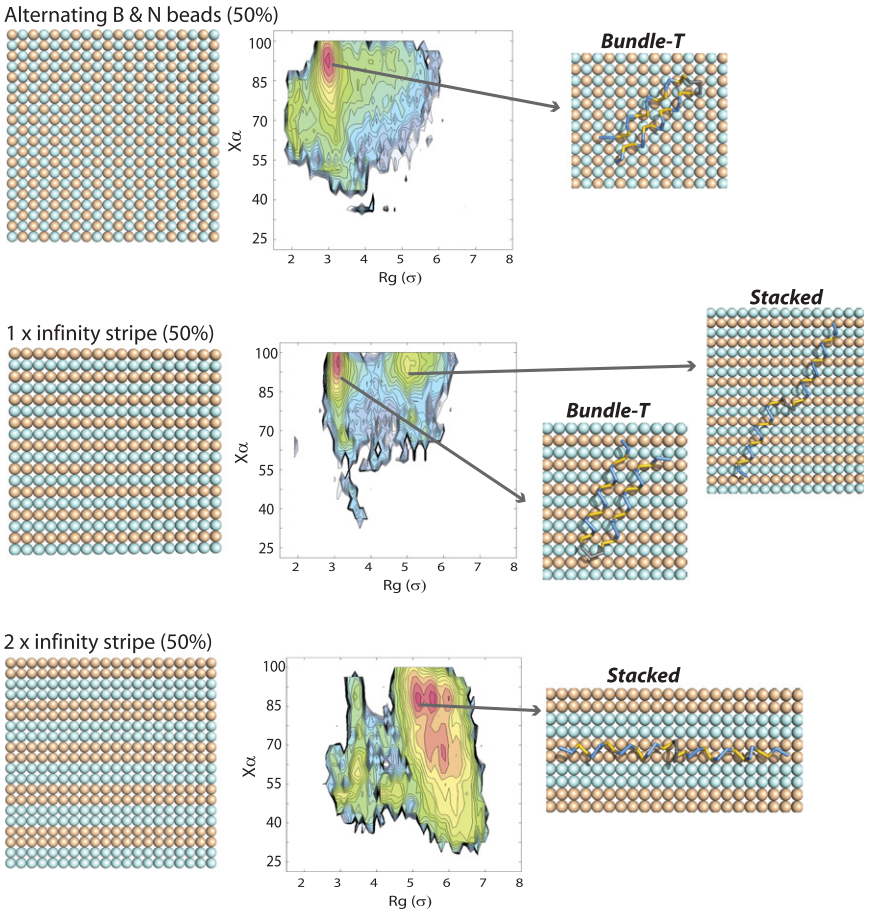

FIGURE 5 Highly hydrophobic (= 50%) explicit surface patterns and their corresponding free-energy maps for the helical peptide model. Free energies are plotted at T = 0.3 (ε/k_B). Top: The alternating B & L pattern at 50%. Helix-coil-helix structures are observed. Middle: 1 × infinity stripe pattern at 50%. Both helix-coil-helix structures (majority) and stacked helical structures (minority) are observed. Bottom: The 2 × infinity stripe pattern at 50%. Stacked helical structures and extended disordered structures are observed. Snapshots are provided for significant minima seen on the free-energy landscapes.

tertiary conformers (i.e., by forming stacked helices instead of helix-coil-helix). In other words, a surface with the correct pattern can strongly bind to and influence folding by complementing solvent-exposed hydrophobic residues on the protein surface.

On the other hand, strongly attractive surfaces (50% hydrophobic beads) are more likely to bind to proteins nonspecifically and, in principle, can both stabilize them through planar confinement and destabilize them by competing with and disrupting native intramolecular interactions. Protein adhesion/adsorption can stabilize the native state indirectly by reducing the entropy of the unfolded state (53–58). However, strong peptide surface interactions can also destabilize a protein by competing with the formation of native tertiary intramolecular interactions, causing the protein to fall apart in an effort to bring its residues in contact with the surface (53). A number of theoretical coarse-grained models have been used to illustrate how an attractive surface can denature proteins (53,58–62). Some proteins, such as fibrinogen, are known to be denatured in the presence of a hydrophobic surface (63,64). However, the two peptide models considered here share certain key characteristics (specifically, simpler topologies and limited intramolecular interactions) with intrinsically disordered proteins. Thus, destabilization by competing interactions upon surface binding was rarely observed in our study. In fact, the peptides in our study were stabilized by a continuous hydrophobic surface. Our results are consistent with earlier findings that a hydrophobic surface (e.g., Teflon) can promote helix formation in small peptides, such as the amyloid β-protein (65,66). In general, a wide variety of strongly attractive/hydrophobic surfaces can influence protein folding because the binding is nonspecific. The pattern on the surface does not have to complement the protein that is bound to it. A pattern consisting of alternating stripes (1 × infinity stripe at 50%) appears to have similar effect on peptide folding compared with a pattern of alternating B and N beads at 50% (Fig. 5).

In the helical model, we find that surfaces with low hydrophobicity almost exclusively utilize pattern recognition to encourage the peptide to fold into helices. Consequently, it is more essential to choose the right pattern at low hydrophobicity. At higher hydrophobicity, the surface may encourage folding in two different ways: 1), by facilitating pattern recognition; or 2), by providing a more amiable environment and reducing the need to bury hydrophobic residues. As a result, higher surface hydrophobicity may

compensate for the imperfection of the pattern, thus allowing the unfavorable pattern (e.g., 1 × infinity single stripe) to become favorable. Because binding can occur anywhere on the high-hydrophobicity surface (due to higher surface coverage of hydrophobic beads) and does not always require pattern recognition, we are able to observe multiple stable conformers on a given surface. This is different from what is observed on a surface with low hydrophobicity, where specific binding tends to favor only one stabilized conformer. For example, it is possible to favor how the two helices are positioned with respect to each other on an explicit surface at low hydrophobicity by simply varying the pattern, as can be seen in the example of the 2 × 9 stripe versus 2 × infinity stripe pattern. On explicit surfaces with high hydrophobicity (1 × infinity stripe at 50%), the free-energy map will show basins for both helix-coil-helices (more favored) and stacked helix conformers (less favored) instead of just one of the two. Due to the lack of pattern on the continuous surfaces, we were not able to control the tertiary arrangement of the two helices (i.e., bundle versus stacked). As the overall hydrophobicity on continuous surfaces increases, the peptide folds into a homogeneous population of helix-coil-helices. The bundle conformer is favored on the continuous surface because it allows a higher number of intramolecular interactions (helix-helix interactions) while still retaining the same number of intermolecular interactions (helix-surface interactions) as the stacked conformer. On the explicit surface, it is possible to favor the stacked conformer because the availability of the helix-surface interaction can be easily modified with the use of patterns.

It is worth mentioning that the helix-coil-helix conformers obtained on the explicit and continuous surfaces are slightly different (Fig. S5). The conformers obtained on the continuous surfaces do not closely resemble those found in the four-helix bundle. Both the 1 × 9 and 2 × 9 explicit rectangle patterns are narrow, which causes the hydrophobic residues from the two neighboring helices to face each other, in similarity to the type of packing expected in a four-helix bundle (Fig. 2, dimer). This is not surprising, because these surfaces were designed to mimic the missing portion of the four-helix bundle that was removed. On the other hand, the helix-coil-helix conformers on the continuous surfaces are more flattened, and thus the hydrophobic residues face the surface instead of facing other hydrophobic residues in the neighboring helix. Our results suggest that, compared with continuous surfaces, explicit surface patterns allow a higher degree of control in terms of guiding peptide folding. Of interest, however, when we widened the 2 × 9 rectangle pattern to a 3 × 9 pattern in an attempt to relax the packing in the helix-coil-helix so that it would become more flattened (as seen on the continuous surface), we found that most of the structures instead became completely disordered, highlighting the sensitivity and specificity of pattern recognition.

CONCLUSIONS

In nature, protein-protein and protein-surface interactions are driven by both specific and nonspecific associations. Generic, nonspecific attraction leads to binding and can stabilize (or destabilize) protein structure and even catalyze folding. In this respect, pattern recognition is not a requirement for protein binding and assisted folding. However, in this work we have demonstrated that pattern recognition can significantly enhance protein binding and folding for a simple model protein. Surfaces with patterns that complement their target proteins can bind to and stabilize them more effectively than surfaces with nonspecific, noncomplementary patterns. A pattern can be designed to trigger drastic conformational rearrangement in a protein, even if the surface makes a comparatively small number of attractive interactions with the protein (i.e., even if the surface has low average hydrophobicity). It would be interesting to explore further examples of surface interfaces with low average hydrophobicity/affinity using multiple model proteins with different folds. Our studies suggest that it would be feasible to tune the patterns and hydrophobicity of the binding interface to attain high specificity.

Finally, this work lays the framework for addressing binding of intrinsically disordered proteins as well. The pattern on a surface can be considered as patches representing a binding site in a larger protein. As shown above, the correct patterns in a binding interface can help the surface recover the right conformation of a binding partner (ligand). This kind of mechanism may be applicable to the coupled folding and binding events associated with intrinsically disordered proteins or peptides. This is especially relevant in the case of intrinsically disordered proteins that adopt different conformations when binding to different partners. Our simulations provide an example of how changes in patterns between different binding partners can induce different folded conformations for the same intrinsically disordered segment.

SUPPORTING MATERIAL

Six figures are available at http://www.biophysj.org/biophysj/supplemental/S0006-3495(11)00038-5.

This research was funded by the David and Lucile Packard Foundation, the National Science Foundation (MCB-0642088), and the Institute for Multiscale Materials Studies, University of California-Santa Barbara/Los Alamos National Laboratory .

REFERENCES

1. Hazy, E., and P. Tompa. 2009. Limitations of induced folding in molecular recognition by intrinsically disordered proteins. *ChemPhysChem.* 10:1415–1419.
2. Dunker, A. K., I. Silman, …, J. L. Sussman. 2008. Function and structure of inherently disordered proteins. *Curr. Opin. Struct. Biol.* 18:756–764.

3. Dyson, H. J., and P. E. Wright. 2005. Intrinsically unstructured proteins and their functions. *Nat. Rev.* 6:197–208.
4. Galea, C. A., Y. Wang, …, R. W. Kriwacki. 2008. Regulation of cell division by intrinsically unstructured proteins: intrinsic flexibility, modularity, and signaling conduits. *Biochemistry.* 47:7598–7609.
5. Tompa, P. 2005. The interplay between structure and function in intrinsically unstructured proteins. *FEBS Lett.* 579:3346–3354.
6. Almeida, P. F., and A. Pokorny. 2009. Mechanisms of antimicrobial, cytolytic, and cell-penetrating peptides: from kinetics to thermodynamics. *Biochemistry.* 48:8083–8093.
7. Latour, R. A. 2008. Molecular simulation of protein-surface interactions: benefits, problems, solutions, and future directions. *Biointerphases.* 3:FC2–FC12.
8. Rea, A. M., V. Thurston, and M. S. Searle. 2009. Mechanism of ligand-induced folding of a natively unfolded helixless variant of rabbit I-BABP. *Biochemistry.* 48:7556–7564.
9. Kohn, J. E., and K. W. Plaxco. 2005. Engineering a signal transduction mechanism for protein-based biosensors. *Proc. Natl. Acad. Sci. USA.* 102:10841–10845.
10. Kouvatsos, N., J. K. Meldrum, …, N. R. Thomas. 2006. Coupling ligand recognition to protein folding in an engineered variant of rabbit ileal lipid binding protein. *Chem. Commun. (Camb.).* 44:4623–4625.
11. Oh, K. J., K. J. Cash, and K. W. Plaxco. 2009. Beyond molecular beacons: optical sensors based on the binding-induced folding of proteins and polypeptides. *Chemistry.* 15:2244–2251.
12. Brunel, F. M., M. B. Zwick, …, P. E. Dawson. 2006. Structure-function analysis of the epitope for 4E10, a broadly neutralizing human immunodeficiency virus type 1 antibody. *J. Virol.* 80:1680–1687.
13. Oh, K. J., K. J. Cash, and K. W. Plaxco. 2006. Excimer-based peptide beacons: a convenient experimental approach for monitoring polypeptide-protein and polypeptide-oligonucleotide interactions. *J. Am. Chem. Soc.* 128:14018–14019.
14. Oh, K. J., K. J. Cash, …, K. W. Plaxco. 2007. Peptide beacons: a new design for polypeptide-based optical biosensors. *Bioconjug. Chem.* 18:607–609.
15. Oldfield, C. J., J. Meng, …, A. K. Dunker. 2008. Flexible nets: disorder and induced fit in the associations of p53 and 14-3-3 with their partners. *BMC Genomics.* 9 (*Suppl 1*):S1.
16. Sivaraman, B., and R. A. Latour. 2010. The adherence of platelets to adsorbed albumin by receptor-mediated recognition of binding sites exposed by adsorption-induced unfolding. *Biomaterials.* 31:1036–1044.
17. Sivaraman, B., and R. A. Latour. 2010. The relationship between platelet adhesion on surfaces and the structure versus the amount of adsorbed fibrinogen. *Biomaterials.* 31:832–839.
18. Castells, V., S. Yang, and P. R. Van Tassel. 2002. Surface-induced conformational changes in lattice model proteins by Monte Carlo simulation. *Phys. Rev. E Stat. Nonlin. Soft Matter Phys.* 65:031912.
19. Maste, M. C. L., W. Norde, and A. J. W. G. Visser. 1997. Adsorption-induced conformational changes in the serine proteinase savinase: a tryptophan fluorescence and circular dichroism study. *J. Colloid Interface Sci.* 196:224–230.
20. Mollmann, S. H., J. T. Bukrinsky, …, U. Elofsson. 2005. Adsorption of human insulin and AspB28 insulin on a PTFE-like surface. *J. Colloid Interface Sci.* 286:28–35.
21. Mollmann, S. H., L. Jorgensen, …, S. Frokjaer. 2006. Interfacial adsorption of insulin conformational changes and reversibility of adsorption. *Eur. J. Pharm. Sci.* 27:194–204.
22. Blanco, F. J., G. Rivas, and L. Serrano. 1994. A short linear peptide that folds into a native stable β-hairpin in aqueous solution. *Nat. Struct. Biol.* 1:584–590.
23. Gellman, S. H. 1998. Minimal model systems for β sheet secondary structure in proteins. *Curr. Opin. Chem. Biol.* 2:717–725.
24. Muñoz, V., P. A. Thompson, …, W. A. Eaton. 1997. Folding dynamics and mechanism of β-hairpin formation. *Nature.* 390:196–199.
25. Ramírez-Alvarado, M., T. Kortemme, …, L. Serrano. 1999. β-Hairpin and β-sheet formation in designed linear peptides. *Bioorg. Med. Chem.* 7:93–103.
26. Kamtekar, S., and M. H. Hecht. 1995. Protein motifs. 7. The four-helix bundle: what determines a fold? *FASEB J.* 9:1013–1022.
27. West, M. W., and M. H. Hecht. 1995. Binary patterning of polar and nonpolar amino acids in the sequences and structures of native proteins. *Protein Sci.* 4:2032–2039.
28. Xiong, H., B. L. Buckwalter, …, M. H. Hecht. 1995. Periodicity of polar and nonpolar amino acids is the major determinant of secondary structure in self-assembling oligomeric peptides. *Proc. Natl. Acad. Sci. USA.* 92:6349–6353.
29. Dodson, C. A., N. Ferguson, …, A. R. Fersht. 2010. Engineering a two-helix bundle protein for folding studies. *Protein Eng. Des. Sel.* 23:357–364.
30. Hill, R. B., D. P. Raleigh, …, W. F. DeG]\rado. 2000. De novo design of helical bundles as models for understanding protein folding and function. *Acc. Chem. Res.* 33:745–754.
31. Dunker, A. K., C. J. Oldfield, …, V. N. Uversky. 2008. The unfoldomics decade: an update on intrinsically disordered proteins. *BMC Genomics.* 9 (*Suppl 2*):S1.
32. Gunasekaran, K., C. J. Tsai, …, R. Nussinov. 2003. Extended disordered proteins: targeting function with less scaffold. *Trends Biochem. Sci.* 28:81–85.
33. Kriwacki, R. W., L. Hengst, …, P. E. Wright. 1996. Structural studies of p21Waf1/Cip1/Sdi1 in the free and Cdk2-bound state: conformational disorder mediates binding diversity. *Proc. Natl. Acad. Sci. USA.* 93:11504–11509.
34. Bellesia, G., A. I. Jewett, and J. E. Shea. 2010. Sequence periodicity and secondary structure propensity in model proteins. *Protein Sci.* 19:141–154.
35. Guo, Z., and D. Thirumalai. 1996. Kinetics and thermodynamics of folding of a de novo designed four-helix bundle protein. *J. Mol. Biol.* 263:323–343.
36. Honeycutt, J. D., and D. Thirumalai. 1990. Metastability of the folded states of globular proteins. *Proc. Natl. Acad. Sci. USA.* 87:3526–3529.
37. Honeycutt, J. D., and D. Thirumalai. 1992. The nature of folded states of globular proteins. *Biopolymers.* 32:695–709.
38. Nozaki, Y., and C. Tanford. 1971. The solubility of amino acids and two glycine peptides in aqueous ethanol and dioxane solutions. Establishment of a hydrophobicity scale. *J. Biol. Chem.* 246:2211–2217.
39. Tanford, C. 1962. Contribution of hydrophobic interactions to the stability of the globular conformation of proteins. *J. Am. Chem. Soc.* 84:4240–4247.
40. Wolfenden, R. 2007. Experimental measures of amino acid hydrophobicity and the topology of transmembrane and globular proteins. *J. Gen. Physiol.* 129:357–362.
41. Wolfenden, R., L. Andersson, …, C. C. Southgate. 1981. Affinities of amino acid side chains for solvent water. *Biochemistry.* 20:849–855.
42. Baumketner, A., A. Jewett, and J. E. Shea. 2003. Effects of confinement in chaperonin assisted protein folding: rate enhancement by decreasing the roughness of the folding energy landscape. *J. Mol. Biol.* 332: 701–713.
43. Earl, D. J., and M. W. Deem. 2005. Parallel tempering: theory, applications, and new perspectives. *Phys. Chem. Chem. Phys.* 7:3910–3916.
44. Sugita, Y., and Y. Okamoto. 1999. Replica-exchange molecular dynamics method for protein folding. *Chem. Phys. Lett.* 314:141–151.
45. Swendsen, R. H., and J. S. Wang. 1986. Replica Monte Carlo simulation of spin glasses. *Phys. Rev. Lett.* 57:2607–2609.
46. Reference deleted in proof.
47. Ferrenberg, A. M., and R. H. Swendsen. 1988. New Monte Carlo technique for studying phase transitions. *Phys. Rev. Lett.* 61:2635–2638.
48. Ferrenberg, A. M., and R. H. Swendsen. 1989. Optimized Monte Carlo data analysis. *Phys. Rev. Lett.* 63:1195–1198.

49. Kumar, S., D. Bouzida, …, J. M. Rosenberg. 1992. The weighted histogram analysis method for free-energy calculations on biomolecules. I. The method. *J. Comput. Chem.* 13:1011–1021.

50. Glykos, N. M., G. Cesareni, and M. Kokkinidis. 1999. Protein plasticity to the extreme: changing the topology of a 4-α-helical bundle with a single amino acid substitution. *Structure.* 7:597–603.

51. Hill, R. B., and W. F. DeGrado. 1998. Solution structure of α_2D, a nativelike de novo designed protein. *J. Am. Chem. Soc.* 120:1138–1145.

52. O'Brien, E. P., G. Stan, …, B. R. Brooks. 2008. Factors governing helix formation in peptides confined to carbon nanotubes. *Nano Lett.* 8:3702–3708.

53. Chan, H. S., and K. A. Dill. 1996. A simple model of chaperonin-mediated protein folding. *Proteins.* 24:345–351.

54. Mittal, J., and R. B. Best. 2008. Thermodynamics and kinetics of protein folding under confinement. *Proc. Natl. Acad. Sci. USA.* 105:20233–20238.

55. Takagi, F., N. Koga, and S. Takada. 2003. How protein thermodynamics and folding mechanisms are altered by the chaperonin cage: molecular simulations. *Proc. Natl. Acad. Sci. USA.* 100:11367–11372.

56. Thirumalai, D., D. K. Klimov, and G. H. Lorimer. 2003. Caging helps proteins fold. *Proc. Natl. Acad. Sci. USA.* 100:11195–11197.

57. Zhou, H. X., and K. A. Dill. 2001. Stabilization of proteins in confined spaces. *Biochemistry.* 40:11289–11293.

58. Sharma, S., B. J. Berne, and S. K. Kumar. 2010. Thermal and structural stability of adsorbed proteins. *Biophys. J.* 99:1157–1165.

59. Betancourt, M. R., and D. Thirumalai. 1999. Exploring the kinetic requirements for enhancement of protein folding rates in the GroEL cavity. *J. Mol. Biol.* 287:627–644.

60. Jewett, A. I., A. Baumketner, and J. E. Shea. 2004. Accelerated folding in the weak hydrophobic environment of a chaperonin cavity: creation of an alternate fast folding pathway. *Proc. Natl. Acad. Sci. USA.* 101:13192–13197.

61. Lu, D., Z. Liu, and J. Wu. 2006. Structural transitions of confined model proteins: molecular dynamics simulation and experimental validation. *Biophys. J.* 90:3224–3238.

62. Stan, G., G. H. Lorimer, …, B. R. Brooks. 2007. Coupling between allosteric transitions in GroEL and assisted folding of a substrate protein. *Proc. Natl. Acad. Sci. USA.* 104:8803–8808.

63. Balasubramanian, V., N. K. Grusin, …, S. M. Slack. 1999. Residence-time dependent changes in fibrinogen adsorbed to polymeric biomaterials. *J. Biomed. Mater. Res.* 44:253–260.

64. Tang, L., Y. Wu, and R. B. Timmons. 1998. Fibrinogen adsorption and host tissue responses to plasma functionalized surfaces. *J. Biomed. Mater. Res.* 42:156–163.

65. Giacomelli, C. E., and W. Norde. 2003. Influence of hydrophobic Teflon particles on the structure of amyloid β-peptide. *Biomacromolecules.* 4:1719–1726.

66. Giacomelli, C. E., and W. Norde. 2005. Conformational changes of the amyloid β-peptide (1-40) adsorbed on solid surfaces. *Macromol. Biosci.* 5:401–407.